Mixed RF-VLC Relaying Systems for High-Speed Rail Communication

Rupender Singh, *Member, IEEE*, Ijaz Ahmad, *Member, IEEE*, and Jyrki Huusko

***Abstract*—In the proposed system setup, a communication link is established between base station (BS) and end-user (UE) via a relay node mounted on the high-speed train (HST). The information is conveyed over backhaul RF links between BS and relay and over VLC links between relay and UE inside the train. It is assumed that RF links are encountered with dual shadowing due to slow-moving vehicles and pedestrians. Moreover, the relay node is not able to estimate the channel information perfectly due to HST mobility. Firstly, the statistical characteristics, such as the probability density function (PDF) and cumulative distribution function of the BS-relay link, are derived under imperfect channel information. Then, the system performance is examined by deriving the two key metrics, outage probability, and average bit error rate. Furthermore, we investigate the secrecy performance of the proposed system when the RF eavesdropper overhears the link between BS and relay and the VLC eavesdropper captures the information via the relay-UE link. To this end, the secure outage probability is derived into a closed form. Our results reveal that the proposed system setup can be adopted as a network architecture for existing as well as for future HST networks.**

***Index Terms*—Channel state information (CSI), double shadowed rician (DSR) fading, doppler shift, high-speed train (HST), visible light communication (VLC).**

I. Introduction

EXPLOSIVE growth of high-speed trains (HSTs), as well as a huge increase in demand for seamless Internet-based services and other emerging applications (e.g., augmented reality (AR), virtual reality (VR), and video-on-demand), has made the continuous provisioning of high-capacity access networks HST an exciting topic of research. The main objective is to provide a high quality of service (QoS), such as low latency and high data rates, to a large number of passengers crowded on the HST at train speeds of up to 500 kmph, similar to low mobility users (or pedestrian users) [1]. On the other hand, the high speed of HST causes serious problems such as the Doppler effect and penetration loss due to train coaches, limiting the QoS of mobile users. Therefore, traditional techniques, including mobile relay-based network architecture [2], beamforming, multiple-input multiple-output (MIMO) [3], and optical wireless communication (OWC) are proposed as promising solutions for HST communication to handle high- data traffic and improve QoS since the first launch of HSTs.

Researchers are also actively working towards standardization of fifth-generation (5G) new radio (NR) for HST communication under the Third Generation Partnership Project (3GPP) with less than 1 ms latency at 500 km/s [4]. Today onboard passengers require a large amount of data services to run different applications, including internet services, online gaming, and high-definition videos. The other applications, such as train collision avoidance systems and surveillance cameras, also require a high data rate. In other words, if 500 passengers on the HST are accessing data connectivity at 2 Mbps, then 1 Gbps data speed is required to serve them [5]. The current 5G technologies are incapable of meeting such huge demand and are limited to providing a maximum of 100 Mbps connectivity [6].

The emerging technologies in 5G are introduced for HST communication to handle the demand of high-speed internet and attract more attention nowadays. These wireless technologies can play a significant role in providing a high-quality user experience and guaranteeing safe operation [7], [8], [9], [10], [11], [12], [13]. Particularly, the OWC technology for indoor and outdoor applications in 5G networks can be utilized as a hopeful solution to support more users with high data rates, offering other benefits such as license-free and low cost. In [14], a novel free-space optical (FSO) technique was proposed to enhance the performance of HST communication by utilizing reconfigurable intelligent surfaces (RIS). In [15], a sequence blind detection method was presented for FSO-based HST systems. The authors in [16], [17] investigated the outage performance of backhaul HST systems based on the unmanned aerial vehicle (UAV) mounted FSO. The focus of these works is limited to studying the FSO-based HST system. On the other hand, in recent years, many research communities have advocated that visible light communication (VLC) has a high proficiency in serving as a communication link between two nodes. Simultaneously, VLC systems are also used for illumination as it works in the visible spectrum region (i.e., 380–750 nm wavelengths). Moreover, the VLC links are also considered RF interference immune and hence, suitable for "interference-sensitive" applications [18]. Therefore, RF technologies can be adopted as backhaul for outdoor BS-relay links, whereas VLC can be used inside the train to serve onboard passengers [19].

In the proposed relay-based HST system, the base station (BS)-relay link adopts a 2.45 GHz frequency band while nanometer Wave frequency is used for the relay-end user

Manuscript received 22 May 2023; revised 17 July 2023; accepted 4 August 2023. Date of publication 8 August 2023; date of current version 29 August 2023. This work was supported in part by Business Finland through SUNSET-6G and in part by AI-NET-ANTILLAS Projects. *(Corresponding author: Rupender Singh.)*

The authors are with the VTT Technical Research Center of Finland, 02044 Espoo, Finland (e-mail: rsingh1@ec.iitr.ac.in; ijaz.ahmad@vtt.fi; jyrki.huusko@vtt.fi).

Digital Object Identifier 10.1109/JPHOT.2023.3303362

(UE) link, which is emerging as a key technology in 5G. The mobile relay architecture has several benefits over direct HST communication between the BS and the UE. The first benefit is broad coverage with enough power to support the multiple antenna relay for HST communication. Secondly, it provides the opportunity to utilize the indoor VLC frequency band to serve a large number of users in a static environment. Moreover, the mobile relay HST system provides the advantage of channel estimation at the mobile relay instead of UE, which reduces the Doppler shift effect and improves the system reliability.

A. Literature Overview

In the literature, several efforts have been devoted to study the mobile relay networks [20], [21], [22], [23], [24], [25]. In [20], [21], massive MIMO systems were studied. The first-order Gauss-Markov Rayleigh fading channel model is used to characterize the channel aging in [20], whereas a single-cell urban scenario was considered [21]. The impact of mobility on system performance (i.e., average bit-error-rate (BER) and outage) was determined in [22] for both amplify and forward (AF) and decode-and-forward (DF) relaying by adopting an autoregressive model over a fast-fading channel. The authors in [23] adopted a random waypoint (RWP) mobility model to study the mobile wireless network over a generalized η-μ fading channel. In [24], the impact of channel state information (CSI) on mobile relay-based dual-hop RF-VLC network was studied in which the source-relay link was assumed as Nakagami-m distributed while VLC was used to model relay-UE link. Furthermore, the authors in [25], [26] proposed the random direction (RD) mobility model to investigate cooperative HST communication over Nakagami-m and generalized κ-μ fading channels, respectively.

On the other hand, a few studies suggest a cryptographic encryption mechanism to secure the transmission between the BS and the train [27], [28]. However, it has been proved that the eavesdroppers can overhear encrypted messages if chip processing is achieved and the codebook is acquired. Physical Layer Security (PLS) has recently surfaced as a promising approach for achieving perfect secrecy in wireless communication systems. By capitalizing on the stochastic nature and time-varying characteristics of wireless channels, PLS eliminates the need for a secret key, as supported by reference [29]. Rather than relying on traditional encryption techniques, the PLS can be applied to HST systems to improve the safety of train transportation by securing the train control messages.

PLS has been extensively analyzed in literature for various relay-based dual-hop communication systems such as mixed RF-FSO, FSO-RF, RF-VLC, and VLC-RF, as evidenced by numerous studies [30], [31], [32], [33], [34], [35], [36], [37], [38], [39]. Specifically, [30] and [31] proposed simultaneous wireless information and power transfer (SWIPT) based dual-hop mixed RF-FSO and mixed FSO-RF systems, respectively, utilizing power splitting methods and investigating the impact of SWIPT parameters on secrecy performance. On the contrary, several studies [32], [33], [34], [35], [36], [37] have concentrated on analyzing the secrecy performance of RF-VLC and VLC-RF systems. In [32], a dual-hop mixed RF-VLC system was examined under two scenarios: RF-side and VLC-side eavesdropping attacks. Closed-form expressions for the secure outage probability (SOP) and strictly positive secrecy capacity (SPSC) were derived. For a dual-hop mixed VLC-RF system, [33] and [34] determined the SOP in scenarios involving multiple users and an Intelligent Reflecting Surface (IRS), respectively. The impact of light energy harvesting on system security, as indicated by the SOP, was assessed in [35] and [36], where closed-form expressions were provided. Lastly, reference [37] investigated the secrecy performance of a cooperative hybrid VLC-RF system, taking into account the random positions of the relay, legitimate receiver, and eavesdropper in different regions. Moreover, [38] and [39] proposed PLS approaches to secure the transmission link between the BS and HST by applying artificial noise and nonorthogonal multiple access (NOMA) techniques, respectively. However, none of the aforementioned studies address secrecy issues in HST communication that involve mixed RF and VLC links between the BS and UEs. It is noteworthy that transmission over VLC links plays a crucial role in green communication, as it can also be used for illumination purposes simultaneously.

B. Motivation and Contributions

Motivated by the aforementioned studies, the RF and VLC technologies are combined together to develop a relaying system suitable for HST communication. In the proposed system, a relay mounted on the HST serves as an intermediate node between the BS and onboard UEs and receives and transmits the information by exploiting DF relaying scheme. BS transmits signals over a strong line-of-sight (LoS) link with minimal signal scattering. Consequently, the BS-relay link can be represented by a double-shadowed Rician (DSR) fading distribution, which has been demonstrated to be highly effective in modelling strong line-of-sight (LoS) propagation with minimal scattering. Another reason for choosing the DSR fading distribution for the BS-relay link is that it can capture the effects of slow-moving vehicles and pedestrians on the LoS path. Moreover, the DSR distribution can be used to characterize the realistic channels in the frequency band of 2.45 GHz, which is a key technique for long-term evolution (LTE) [5], [6], [7], [8], [9]. It also describes different fading scenarios as special cases for which the values of fading parameters can be found in [31, Table II]. The relay has the capability of converting RF signals into optical signals and transferring the information over the VLC link, which is established between the relay and the UE. This means that the proposed system employs a dual-hop communication scheme where the relay receives an RF signal from the BS and converts it into an optical signal using the DF strategy, which is then transmitted to the onboard UE. The primary contribution of this paper is the introduction of a mixed RF-VLC system for HST communication. Specifically, the system performance under outdated CSI at the relay is examined, with a focus on

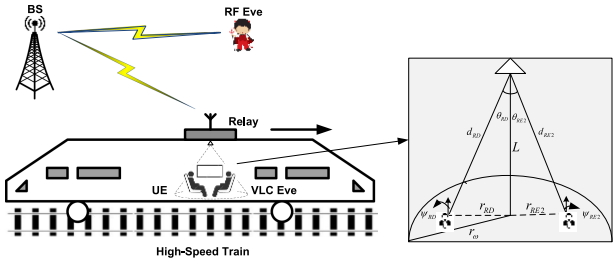

Fig. 1. Proposed dual-hop mixed RF-VLC HST system model.

the impact of BS power and fading parameters on the system's overall performance. In summary:

1) A mixed RF-VLC relaying system is proposed for HST communication where a relay mounted on HST is connected with BS via RF link and onboard UE via VLC link. Note that the 2.45 GHz frequency DSR fading characterizes the BS-relay link, while the relay and UE establish a VLC transmission link.
2) Different from [25], [26], the impact of train mobility is described by the outdated CSI at the relay. The estimated channel information is used to derive statistical characteristics, such as the probability density function (PDF) of the received instantaneous SNR at the relay. The derived results facilitate obtaining the closed-form expressions for outage probability (OP) and average BER. Additionally, further insights are revealed by deriving the asymptotic outage at high large light-emitting diode (LED) power and BS power.
3) Different from [24], [25], [26], [27], [28], [29], [30], [31], [32], [33], [34], [35], [36], [37], a relay-based mixed RF-VLC system for HSTs is studied in this work, in which the SOP is derived for end-to-end SNR of the BS-relay-UE link. The results in our work are presented for both assumptions of RF-side and VLC-side eavesdropping attacks.
4) We demonstrate the numerical results to reveal the effects of various system parameters on the performance of the proposed system.

II. System and Channel Model

As shown in Fig. 1, a system setup is developed for HST communication based on a mixed RF-VLC relaying system in which a DF relay *R* receives signals from BS *S* via an RF link and forwards it to the UE *D* over the VLC link. *R* is equipped with a LED that converts electrical signals into optical signals. It is assumed that two adversaries, i.e., *E1* and *E2*, are present on the RF link and VLC link, respectively, where *E1* can hear the RF link, whereas *E2* is capable of overhearing optical signals and positioned close to UE. BS and *E1* are static, while relay, UE, and *E2* are present on the train and moving with HST speed. It is assumed that BS and UE cannot communicate over a direct path due to the obstacles, and hence, BS sends information to UE through a relay mounted on HST. *R* receives signals from BS through an RF link which is decoded and then forwarded to the UE via a VLC link. *R* is capable of converting perfectly 2.45 GHz signals into nanometer Wave signals. We assume that BS-relay and BS-*E1* links experience the quasi-static DSR fading channel. Notably, *E1* and *E2* are not present when performance metrics are derived, while secrecy performance is investigated in the presence of *E1* and *E2*.

A. BS-Relay and BS-E1 Channel Models

BS transmits a message symbol $s^l = [s(1), s(2), \ldots s(l)]$ to UE which is encoded into a codeword $x^n = [x(1), x(2), \ldots x(n)]$. The signal received by *R* is given as [36, Eq. (1)]

$$y_{SR}[i] = \sqrt{P_s}\widehat{h}_{SR}[i]\, x[i] + z_{SR}[i], \tag{1}$$

where P_s is the transmit power at the BS, $\widehat{h}_{SR}$ is denoting the estimated DSR fading coefficients of BS-relay link and z_{SR} denotes zero-mean complex valued Gaussian noise with variance σ^2_{SR}. Since the relay is dynamic and moving with the HST at the same speed, it cannot estimate the channel perfectly. Therefore, the estimated channel gain is outdated and correlated with precise channel gain (i.e., h_{SR}) of BS-relay link, which can be written as

$$\widehat{h}_{SR} = \rho_{SR} h_{SR} + \sqrt{1-\rho^2_{SR}}\varepsilon_{SR}, \tag{2}$$

where ε_{SR} is zero-mean Gaussian random variable with unit variance and is uncorrelated with h_{SR}. ρ_{SR} is the correlation coefficient between $\widehat{h}_{SR}$ and h_{SR} and can be characterized by using Jakes' autocorrelation model as,

$$\rho_{SR} = J_0(2\pi f_D T_s), \tag{3}$$

where $J_0(\bullet)$ is the zeroth order Bessel's function of first kind, T_s denotes the transmitted symbol duration, $f_D = (f_c v/c)$ describes the Doppler shift frequency where f_c is the carrier frequency and c represents the speed of light. Note that if the train is static, $\rho_{SR} = 1$ otherwise, $0 < \rho_{SR} < 1$.

The instantaneous SNR of the BS-relay link can be expressed as

$$\hat{\gamma}_{SR} = \bar{\gamma}_{SR}\left|\hat{h}_{SR}\right|^2, \tag{4}$$

where $\bar{\gamma}_{SR}$ is the average SNR and defined as $\bar{\gamma}_{SR} = \frac{P_s}{\sigma^2_{SR}}$. The PDF and cumulative probability distribution (CDF) of $\hat{\gamma}_{SR}$ are derived in the following Lemma.

Lemma 1: The PDF and CDF of γ_{SR} are obtained as

$$f_{\hat{\gamma}_{SR}}(\gamma) = \begin{cases} \sum_{p=0}^{\infty}\sum_{q=0}^{\infty} C_1 \Omega^{\frac{q+1}{2}} \gamma^{\frac{q-1}{2}} \exp(-\Omega\gamma), & \gamma > 0 \\ 1-\xi, & \gamma = 0 \end{cases} \tag{5}$$

$$F_{\hat{\gamma}_{SR}}(\gamma) = \begin{cases} \sum_{p=0}^{\infty}\sum_{q=0}^{\infty} C_1 G^{1,1}_{1,2}\left[\Omega\gamma \,\middle|\, \begin{matrix} 1 \\ \frac{q+1}{2}, 0 \end{matrix}\right], & \gamma > 0 \\ 1-\xi, & \gamma = 0 \end{cases} \tag{6}$$

where m_s denotes inverse Nakagami-*m* parameter, m_d denotes Nakagami-*m* parameter, k is Rician parameter, $\hat{r}$ is the mean-square value of r, $\Omega = \frac{\hat{r}}{2(1-\rho^2_{SR})\bar{\gamma}_{SR}}$,

$C_1 = \frac{A_{p_{SR}} 2^{q-1} G_{pq}}{\sqrt{pi}\Gamma(q+1)}$, $\xi = \sum_{p=0}^{\infty}\sum_{q=0}^{\infty} C_1 \Gamma(\frac{q+1}{2})$, $G_{pq} = G_{2,1}^{1,2}\left[\frac{2(1+k_{SR})(1-\rho_{SR}^2)}{(m_{s_{SR}}-1)\bar{r}^2\rho_{SR}^2}\middle| \begin{matrix} -m_{s_{SR}}+1, -q+1 \\ p+1 \end{matrix}\right]$, $A_{p_{SR}} = \frac{m_{s_{SR}} k_{SR}^p (m_{d_{SR}})_p (m_{s_{SR}}+1)_p}{(m_{d_{SR}}+k_{SR})^p p!(1)_p \Gamma(m_{s_{SR}}+1+p)} \left(\frac{m_{d_{SR}}}{m_{d_{SR}}+k_{SR}}\right)^{m_{d_{SR}}}$, $\Gamma(\bullet)$ is Gamma function [40, II.3], $G_{p,q}^{m,n}(\bullet)$ denotes Meijer-G function [40, Eq. (8.2.1.1)], and $(a)_n$ denotes Pochhamer symbol [41, Eq. (06.10.02.0001.01)].

Proof: Please see Appendix A.

Remark 1: It can be observed from (6) that OP of BS-relay link occurs zero floor, which is equal to $1-\xi$ at $\overline{\gamma}_{SR} \to \infty$. This is because ξ is independent of $\overline{\gamma}_{SR}$. In other words, $\widehat{h}_{SR}$ is always positive for practical scenarios while ε_{SR} can be negative or positive.

Remark 2: It is worth pointing out that the two-fold infinite summation in (5) and (6) are convergent and can be truncated only for a few terms of (p,q). This can be followed from the theorem that if $\sum_{q=0}^{\infty} a_{pq}$ converges for $q \in \mathrm{N}$ to a non-negative number b_p and $\sum_{p=0}^{\infty} b_p$ converges for $p \in \mathrm{N}$, then $\sum_{p=0}^{\infty}\sum_{q=0}^{\infty} |a_{pq}|$ also converges for a finite number of (p,q). One can apply the d'Alembert's ratio test to testify to the convergence of infinite series representation of (5) and (6). Therefore, we require only a finite number of terms to achieve the high-precision sum results. For instance, the test for the convergence of the series in (6) is available in Appendix B.

Since *E1* is static and hears the transmission between BS and relay, it can estimate perfect channel parameters. Therefore, the received signal at *E1* can be written as [36]

$$y_{SE1}[i] = \sqrt{P_s} h_{SE1}[i]\, x[i] + z_{SE1}[i], \tag{7}$$

where z_{SE1} denotes zero-mean complex valued Gaussian noise with variance σ_{SE1}^2. From (5), the instantaneous SNR of the BS-*E1* link can be written as

$$\gamma_{SE1} = \bar{\gamma}_{SE1} |h_{SE1}|^2, \tag{8}$$

where $\bar{\gamma}_{SE1}$ is the average SNR of the BS-*E1* link and can be defined as $\bar{\gamma}_{SE1} = \frac{P_s}{\sigma_{SE1}^2}$. The PDF and CDF of γ_{SE1} can be written from [31], [(16) and (17)] as, respectively

$$f_{\gamma_{SE1}}(\gamma) = \sum_{p=0}^{\infty} \frac{A_{p_{SE1}}(1+k_{SE1})}{\bar{\gamma}_{SE1}(m_{s_{SE1}}-1)} G_{1,1}^{1,1}\left[\frac{(1+k_{SE1})\gamma}{(m_{s_{SE1}}-1)\bar{\gamma}_{SE1}}\middle| \begin{matrix} -m_{s_{SE1}} \\ p \end{matrix}\right], \tag{9}$$

$$F_{\gamma_{SE1}}(\gamma) = \sum_{p=0}^{\infty} A_{p_{SE1}} G_{2,2}^{1,2}\left[\frac{(1+k_{SE1})\gamma}{(m_{s_{SE1}}-1)\bar{\gamma}_{SE1}}\middle| \begin{matrix} 1-m_{s_{SE1}}, 1 \\ p+1, 0 \end{matrix}\right], \tag{10}$$

where $A_{p_{SE1}}$ can be obtained from $A_{p_{SR}}$ by replacing $\{m_{s_{SR}}, m_{d_{SR}}, k_{SR}\}$ from $\{m_{s_{SE1}}, m_{d_{SE1}}, k_{SE1}\}$.

B. VLC Channel Model

Inside the HST, the signals received at the UE and *E2* are given as

$$y_t = h_t x' + z_t, \tag{11}$$

where $t \in \{RD, RE2\}$, x' is the non-negative emitted intensity by the LED, which is upper bounded as $E[x'] = P_{opt}$ due to safety concerns, P_{opt} is the transmitted optical power and z_t denotes mean zero complex valued Gaussian noise with variance σ_t^2.

The end users (i.e., *D* and *E2*) are illuminated by the LED source at illumination angle ψ_t and irradiance angle θ_t and positioned at a height L from the receiving plane, as shown in Fig. 1. The location of the end users (i.e., *D* and *E2*) can be determined with the help of Euclidean distance d_t, angle φ_t and radius r_t on the polar coordinate plane.

In indoor VLC subsystem, the channel gain of the tth link can be written from [24] as

$$h_t = \frac{\Lambda_t(\omega+1)\Re}{2\pi d_t^2} \cos^{\omega}(\theta_t)\, T g_t \cos(\psi_t), \tag{12}$$

where Λ denotes the physical area of the photodetector, T represents the optical filter gain, g is the photodetector's concentrator gain, which is related to the field of view (FOV) of the receiver Ψ and refractive index of the lens ζ as $g = \zeta^2/\sin^2(\Psi)$, for $0 \le \psi_t \le \Psi$. $\Re$ describes photodetector's responsivity. $\omega = -1/\log_2(\cos(\phi_{1/2}))$ is the Lambert index which is related to semi-angle of LED $\phi_{1/2}$. Moreover, it is postulated that the surface plane of the photodetector is oriented parallel to the ground plane, then $\theta_t = \psi_t$, $d_t = \sqrt{r_t^2 + L^2}$, and $\cos(\theta_t) = \frac{L}{\sqrt{r_t^2+L^2}}$. Then, (12) can be expressed as

$$h_t = \frac{\chi_t}{(r_t^2 + L^2)^{\frac{\omega+3}{2}}}, \tag{13}$$

where $\chi_t = \frac{\Lambda_t(\omega+1)\Re}{2\pi} T g_t L^{\omega+1}$. The position of the tth user can be characterized using uniform distribution, therefore, PDF of r_t is expressed as $f_{r_t}(r) = \frac{2r}{r_\omega^2}$. Thus, the PDF of h_t can be derived with the help of change of variable method from (13) as

$$f_{h_t}(h_t) = \frac{2\chi_t^{\frac{2}{\omega+3}}}{r_\omega^2(\omega+3)} h_t^{-\frac{\omega+5}{\omega+3}}, \quad h_{t_{\min}} \le h_t \le h_{t_{\max}}, \tag{14}$$

where $h_{t_{\min}} = \chi_t/(r_\omega^2 + L^2)^{\frac{\omega+3}{2}}$ and $h_{t_{\max}} = \chi_t/L^{\omega+3}$. The PDF and CDF of the corresponding SNR can be obtained from (14) as follows

$$f_{\gamma_t}(\gamma) = \frac{(\mu_t \chi_t^2)^{\frac{1}{\omega+3}}}{r_\omega^2(\omega+3)} \gamma^{-\frac{\omega+4}{\omega+3}}, \quad \gamma \in C_3, \tag{15}$$

$$F_{\gamma_t}(\gamma) = \begin{cases} 0, & \gamma \in C_2 \\ -\frac{1}{r_\omega^2}\left(\frac{\mu_t\chi_t^2}{\gamma}\right)^{\frac{1}{\omega+3}} + \frac{L^2}{r_\omega^2} + 1, & \gamma \in C_3 \\ 1, & \gamma \in C_4 \end{cases} \tag{16}$$

where $C_2 = [0, \gamma_{t_{\min}}]$, $C_3 = [\gamma_{t_{\min}}, \gamma_{t_{\max}}]$, $C_4 = [\gamma_{t_{\max}}, \infty]$, $\gamma_{t_{\min}} = \mu_t \chi_t^2/(r_\omega^2 + L^2)^{\omega+3}$, $\gamma_{t_{\max}} = \mu_t \chi_t^2/L^{2(\omega+3)}$, and $\mu_t = P_{opt}^2 \eta^2/\sigma_t^2 B$, where η is the electrical to optical conversion efficiency, and B denotes the baseband modulation bandwidth.

III. Performance Analysis

In this section, we investigate the performance of the proposed dual-hop mixed RF-VLC HST system when no eavesdropper is present. It is assumed that DF relaying scheme is utilized, the end-to-end SNR of the relay-UE link, referred to as γ_{eq}, can be written as

$$\gamma_{eq} = \frac{\widehat{\gamma}_{SR}\gamma_{RD}}{\widehat{\gamma}_{SR} + \gamma_{RD} + 1} \cong \min\left(\widehat{\gamma}_{SR}, \gamma_{RD}\right) \tag{17}$$

A. Outage Probability (OP)

Generally, the OP is defined as the probability of an event in which instantaneous SNR γ_{eq} is smaller than the predetermined threshold SNR γ_{th}. Mathematically, OP can be expressed as

$$\begin{aligned} OP\left(\gamma_{th}\right) &= \Pr\left[\min\left(\widehat{\gamma}_{SR}, \gamma_{RD}\right) < \gamma_{th}\right] \\ &= 1 - \Pr\left[\min\left(\widehat{\gamma}_{SR}, \gamma_{RD}\right) \geqslant \gamma_{th}\right] \\ &= 1 - \Pr\left[\widehat{\gamma}_{SR} \geqslant \gamma_{th}\right] \Pr\left[\gamma_{RD} \geqslant \gamma_{th}\right], \end{aligned} \tag{18}$$

Theorem 1: The OP for the dual-hop mixed RF-VLC HST system can be obtained from (18) with some mathematical manipulation as

$$OP\left(\gamma_{th}\right) = \begin{cases} 1 - \xi + F_{\widehat{\gamma}_{SR}}\left(\gamma_{th}\right), & \gamma_{th} \in C_2 \\ 1 - \left(\xi - F_{\widehat{\gamma}_{SR}}\left(\gamma_{th}\right)\right)\left(1 - P_1\right), & \gamma_{th} \in C_3 \\ 1, & \gamma_{th} \in C_4 \end{cases} \tag{19}$$

Proof: By using the (6) and (15), the terms in (18) can be evaluated as following.

$$\Pr\left[\widehat{\gamma}_{SR} \geqslant \gamma_{th}\right] = \xi - \Pr\left[\widehat{\gamma}_{SR} < \gamma_{th}\right] = \xi - F_{\widehat{\gamma}_{SR}}\left(\gamma_{th}\right) \tag{20}$$

$$\Pr\left[\gamma_{RD} \geq \gamma_{th}\right] = \begin{cases} 1 - \int_0^{\gamma_{RD_{\min}}} f_{\gamma_{RD}}\left(\gamma\right) d\gamma, & \gamma_{th} \in C_2 \\ 1 - \int_{\gamma_{RD_{\min}}}^{\gamma_{th}} f_{\gamma_{RD}}\left(\gamma\right) d\gamma, & \gamma_{th} \in C_3 \\ 1 - \int_{\gamma_{RD_{\max}}}^{\infty} f_{\gamma_{RD}}\left(\gamma\right) d\gamma, & \gamma_{th} \in C_4 \end{cases} \tag{21}$$

Using [38, Eq. (2.01.1)], we can achieve

$$\Pr\left[\gamma_{RD} \geq \gamma_{th}\right] = \begin{cases} 1, & \gamma_{th} \in C_2 \\ 1 - P_1, & \gamma_{th} \in C_3 \\ 0, & \gamma_{th} \in C_4 \end{cases}, \tag{22}$$

where $P_1 = \delta\left(\gamma_{RD_{\min}}^{-\frac{1}{\omega+3}} - \gamma_{th}^{-\frac{1}{\omega+3}}\right)$ and $\delta = \left(\mu_{RD}\chi_{RD}^2\right)^{\frac{1}{\omega+3}}/r_\omega^2$.

The proof is completed by substituting (20) and (22) into (19).

Remark 3: For high transmitted BS power i.e., $P_s \to \infty$, it is concluded that $\bar{\gamma}_{SR} \to \infty$. From (19), it becomes evident that in this scenario, the instantaneous SNR at *D* is equivalent to that of the VLC link, i.e., $\gamma_{eq} \approx \gamma_{RD}$. This implies outage performance of the proposed system is independent of the RF backhaul link and can be controlled by the relay-UE link in a high-power regime. The asymptotic OP can be written as

$$OP_{P_s\to\infty}^{\infty} = \begin{cases} 1 - \xi, & \gamma_{th} \in C_2 \\ 1 - \xi\left(1 - P_1\right), & \gamma_{th} \in C_3 \\ 1, & \gamma_{th} \in C_4 \end{cases}, \tag{23}$$

Remark 4: At a high LED power regime, i.e., $P_{opt} \to \infty$, only the BS-relay link remains dominating as the instantaneous SNR of the VLC link reaches its high value, i.e., $\gamma_{RD} \to \infty$. From (19), it is concluded that $\gamma_{eq} \approx \widehat{\gamma}_{SR}$. The OP for $P_{opt} \to \infty$ is determined as

$$OP_{P_{opt}\to\infty}^{\infty} = 1 - \xi + F_{\widehat{\gamma}_{SR}}\left(\gamma_{th}\right) \tag{24}$$

Similar to Remark 3, the asymptotic OP depends on the RF subsystem of the proposed HST system and becomes independent of VLC fronthaul.

B. Average Bit-Error-Rate (BER)

In the DF relay-based systems, the binary modulated data is decoded at the relay and then transferred to the destination after re-encoding. The received data, either at the relay or the destination, is error-free and erroneous. In this case, the decoding at the relay and the destination are independent of each other. Considering the decoding errors at the relay, we derive the average BER expression for the proposed system when binary phase-shift keying (BPSK) or differential BPSK (DBPSK) is applied. The average BER of a wireless system can be written in terms of the CDF of γ_f from [24, Eq. (47)] as

$$P_e^f = \frac{b^a}{2\Gamma\left(a\right)} \int_0^\infty e^{-b\gamma} \gamma^{a-1} F_{\gamma_f}\left(\gamma\right) d\gamma \tag{25}$$

where $f \in (SR, RD)$. The different values of (a, b) parameters are used to define the modulation schemes. For example, $(a, b) = (0.5, 1)$ for BPSK and $(a, b) = (1, 1)$ for DBPSK.

Theorem 2: For the proposed system, the average BER can be expressed considering decoding errors at relay from [39, Eq. (46)] as

$$\overline{P_e} = P_e^{SR}\left(1 - P_e^{RD}\right) + P_e^{RD}\left(1 - P_e^{SR}\right) \tag{26}$$

where P_e^{SR} and P_e^{RD} denote the average BER of the RF and VLC subsystems, respectively, and are derived in (27) and (28).

Proof: By substituting (6) into (25) and using [40, Eq. (8.4.3.1)], [41, Eq. (07.34.21.0011.01)] and [42, Eq. (3.381)], P_e^{SR} can be obtained as

$$P_e^{SR} = \frac{1}{2\Gamma\left(a\right)} \sum_{p=0}^{\infty} \sum_{q=0}^{\infty} C_1 G_{2,2}^{1,2}\left[\frac{\Omega}{b} \middle| \begin{matrix} 1, 1-a \\ \frac{q+1}{2}, 0 \end{matrix}\right] + \frac{1-\xi}{2} \tag{27}$$

On substituting (16) into (25) and making the use of [40, Eq. (8.2.32)], P_e^{RD} is determined into closed-form as

$$P_e^{RD} = \frac{\Gamma\left(a, b\gamma_{RD_{\max}}\right)}{2\Gamma\left(a\right)} + \frac{1 + \frac{L^2}{r_\omega^2}}{2\Gamma\left(a\right)} z_1 - \frac{\left(b\mu_{RD}\chi_{RD}^2\right)^{\frac{1}{\omega+3}}}{2\Gamma\left(a\right) r_\omega^2} z_2 \tag{28}$$

where $z_1 = \Gamma(a, b\gamma_{RD_{\min}}) - \Gamma(a, b\gamma_{RD_{\max}})$, $z_2 = \Gamma(a - \frac{1}{\omega+3}, b\gamma_{RD_{\min}}) - \Gamma(a - \frac{1}{\omega+3}, b\gamma_{RD_{\max}})$.

Remark 5: One can obtain the average BER for a mixed RF-VLC HST system considering perfect relaying or error-free

decoding at the relay by subtitling the CDF of γ_{eq} into (25). The CDF of γ_{eq} can be written as

$$F_{\gamma_{eq}}(\gamma) = F_{\widehat{\gamma}_{SR}}(\gamma) + F_{\gamma_{RD}}(\gamma) - F_{\widehat{\gamma}_{SR}}(\gamma) F_{\gamma_{RD}}(\gamma),$$

where $F_{\widehat{\gamma}_{SR}}(\gamma)$ and $F_{\gamma_{RD}}(\gamma)$ are given in (6) and (16), respectively.

Remark 6: Similar to OP, the asymptotic expressions for average BER can be obtained for $P_s \to \infty$ and $P_{opt} \to \infty$ in (29) and (30), respectively.

$$\overline{P}_e^{P_s \to \infty} = \frac{1-\xi}{2} + P_e^{RD}\xi \tag{29}$$

$$\overline{P}_e^{P_{opt} \to \infty} = P_e^{SR} \tag{30}$$

IV. Physical Layer Security Analysis

In this section, we derive the SOP by considering the presence of active eavesdroppers on BS-relay link and relay-UE link, respectively. For this scenario, the security is compromised if the instantaneous secrecy capacity i.e., C_o is less than the predefined constant rate i.e., R_o and otherwise perfect secrecy is achieved. As the proposed system is utilizing the DF relaying protocol, the capacity of the system is dominated by the worst hop and expressed as

$$C_o = \min(C_{SR}, C_{RD}), \tag{31}$$

where C_{SR} and C_{RD} present the capacity of BS-relay and relay-UE links, respectively. One of the common and useful secrecy performance metric SOP can be defined as the probability of $C_o \leq R_o$ and is expressed as [30]

$$P_{SOP}(R_o) = \Pr(\min(C_{SR}, C_{RD}) < R_o) \tag{32}$$

Under DF scheme, both links (i.e., BS-relay and relay-UE) are independent of each other. Therefore, (32) can be rewritten by using basic probability theory as

$$\begin{aligned} P_{SOP}(R_o) &= 1 - \Pr(\min(C_{SR}, C_{RD}) \geq R_o) \\ &= 1 - \Pr(C_{SR} \geq R_o, C_{RD} \geq R_o) \\ &= 1 - \Pr(C_{SR} \geq R_o)\Pr(C_{RD} \geq R_o) \end{aligned} \tag{33}$$

where

$$\Pr(C_{SR} \geq R_o) = 1 - \Pr(C_{SR} < R_o) \tag{34}$$

$$\Pr(C_{RD} \geq R_o) = 1 - \Pr(C_{RD} < R_o) \tag{35}$$

A. Eavesdropping on BS-Relay Link

In this case, it is assumed that a static eavesdropper *E1* is present on the BS-relay link and can hear the secure transmission through RF link, then the instantaneous capacity of the BS-relay link can be written as

$$C_{SR} = \frac{1}{2}\left[\log_2(1+\widehat{\gamma}_{SR}) - \log_2(1+\gamma_{SE1})\right] \tag{36}$$

Similarly, the capacity of the second hop can be written from [32] as

$$C_{RD} = \frac{1}{2}\log_2(1+\gamma_{RD}) \tag{37}$$

Theorem 3: The lower bound on SOP for DF mixed RF-VLC HST system can be obtained under the RF eavesdropping attacks as given in (45).

Proof: Substituting (36) into (34), we have

$$\Pr(C_{SR} \geqslant R_o) = 1 - \Pr\left[\frac{1}{2}\log_2\left(\frac{1+\widehat{\gamma}_{SR}}{1+\gamma_{SE1}}\right) \leqslant R_o\right] \tag{38}$$

R_o in (38) can also be represented in terms of predetermined threshold γ_{th} as $R_o = \frac{1}{2}\log_2(1+\gamma_{th})$. (38) further can be expressed in terms of PDF and CDF as

$$\begin{aligned} &\Pr(C_{SR} \geqslant R_o) \\ &= 1 - \int_0^\infty F_{\widehat{\gamma}_{SR}}\left(2^{2R_o}(1+\gamma_{SE1})\right) f_{\gamma_{SE1}}(\gamma_{SE1})\, d\gamma_{SE1} \end{aligned} \tag{39}$$

Since (39) cannot be obtained in exact closed-form, the upper bound of (39) can be derived by utilizing a similar method presented in [32] as follows:

$$\Pr(C_{SR} \geqslant R_o) \leqslant 1 - \int_0^\infty F_{\widehat{\gamma}_{SR}}\left(2^{2R_o}\gamma_{SE1}\right) f_{\gamma_{SE1}}(\gamma_{SE1})\, d\gamma_{SE1} \tag{40}$$

By substituting (6) and (9) into (40) and making use of [41, Eq. (07.34.21.0011.01)], (40) can be obtained in closed-from as

$$\begin{aligned} &\Pr(C_{SR} \geq R_o) \\ &\leq \xi - \sum_{p=0}^{\infty}\sum_{q=0}^{\infty}\sum_{u=0}^{\infty} C_1 A_{u_{SE1}} G_{2,3}^{2,2}\left[\Theta \,\middle|\, \begin{matrix} 1, -u \\ \frac{q+1}{2}, m_{s_{SE1}}, 0 \end{matrix}\right] \end{aligned} \tag{41}$$

where $\Theta = \frac{2R_o\Omega(m_{s_{SE1}}-1)\bar{\gamma}_{SE1}}{(1+k_{SE1})}$.

Now, substituting (37) into (35), we have

$$\Pr(C_{RD} \geq R_o) = 1 - \Pr\left[\frac{1}{2}\log_2\left(1+c^2\gamma_{RD}\right) < R_o\right] \tag{42}$$

From (15) and (42), we have

$$\begin{aligned} &\Pr(C_{RD} \geq R_o) = 1 - \Pr\left(\gamma_{RD} < 2^{2R_o} - 1\right) \\ &= \begin{cases} 1 - \int_0^{\gamma_{RD_{\min}}} f_{\gamma_{RD}}(\gamma)\, d\gamma, & 2^{2R_o} - 1 \in C_2 \\ 1 - \int_{\gamma_{RD_{\min}}}^{2^{2R_o}-1} f_{\gamma_{RD}}(\gamma)\, d\gamma, & 2^{2R_o} - 1 \in C_3 \\ 1 - \int_{\gamma_{RD_{\max}}}^{\infty} f_{\gamma_{RD}}(\gamma)\, d\gamma, & 2^{2R_o} - 1 \in C_4 \end{cases}, \end{aligned} \tag{43}$$

Using [38, (2.01.1)], (43) can be expressed as

$$\Pr(C_{RD} \geq R_o) = \begin{cases} 1, & 2^{2R_o} - 1 \in C_2 \\ 1 - P_3, & 2^{2R_o} - 1 \in C_3 \\ 0, & 2^{2R_o} - 1 \in C_4 \end{cases}, \tag{44}$$

where $P_3 = \delta\left(\gamma_{RD_{\min}}^{-\frac{1}{\omega+3}} - (2^{2R_o}-1)^{-\frac{1}{\omega+3}}\right)$.

Finally, the lower bound on SOP is deduced in (45) by substituting (41) into (44) in (33) as

$$P_{SOP}^{L}\left(R_o\right)=\begin{cases}1-\xi+G_{pqu}, & 2^{2R_o}-1\in C_2\\ 1-\left(\xi-G_{pqu}\right)\left(1-P_3\right), & 2^{2R_o}-1\in C_3\\ 1, & 2^{2R_o}-1\in C_4\end{cases}, \tag{45}$$

where $G_{pqu}=\sum_{p=0}^{\infty}\sum_{q=0}^{\infty}\sum_{u=0}^{\infty}C_1A_{u_{SE1}}G_{2,3}^{2,2}\left[\Theta\middle|\begin{matrix}1,-u\\ \frac{q+1}{2},m_{s_{SE1}},0\end{matrix}\right]$.

Remark 6: It can easily be found from (45) that smaller values of R_o will lead to smaller SOP while the larger values of R_o will result in a larger SOP. This is because, at larger R_o, the possibility of outage occurrence on the relay-UE link will be increased. Therefore, an optimal R_o can be obtained to minimize the SOP and maximize the secrecy throughput by utilizing the root-finding method [43].

Remark 7: Since only the BS-relay link is under eavesdropping attack, the secrecy performance is significantly affected by the variation in Doppler shiftf_DT_s or the speed of HST. The larger f_DT_s leads to higher estimation errors at the relay and hence results in low SNR at the relay. The effects of f_DT_s can be mitigated by varying the values of parameters controlling the relay-UE links, such as FOV and height of LED from the UE L only when $2^{2R_o}-1\in C_3$ otherwise, the secrecy will be compromised with the larger f_DT_s.

Remark 8: Considering the case of $P_s\to\infty$, (41) becomes independent of $\overline{\gamma}_{SR}$ i.e., $\Pr(C_{SR}\geq R_o)\leq\xi$. Therefore, the asymptotic expression for lower bound on SOP can be written from (45) as

$$P_{SOP}^{P_s\to\infty}\left(R_o\right)=\begin{cases}1-\xi, & 2^{2R_o}-1\in C_2\\ 1-\xi+\xi P_3, & 2^{2R_o}-1\in C_3\\ 1, & 2^{2R_o}-1\in C_4\end{cases} \tag{46}$$

Similar to (24) and (30), it can be shown that lower bound on SOP for $P_{opt}\to\infty$ is given by

$$P_{SOP}^{P_{opt}\to\infty}\left(R_o\right)=1-\xi+G_{pqu} \tag{47}$$

B. Eavesdropping on BS-UE Link

This is the case when eavesdropper *E2* is present on the train and wiretapping the relay-UE link. This system setup is similar to the scenario of the indoor VLC system as presented in [24], [32], [37]. In this case, the capacity of the relay-UE link can be expressed as [32]

$$C_{RD}=\frac{1}{2}\left[\log_2\left(1+\gamma_{RD}\right)-\log_2\left(1+\gamma_{SE2}\right)\right] \tag{48}$$

and the capacity of the BS-relay link is given as

$$C_{SR}=\frac{1}{2}\log_2\left(1+\widehat{\gamma}_{SR}\right) \tag{49}$$

Theorem 4: By considering the presence of an eavesdropping attack on the indoor VLC link inside HST, the lower bound of the SOP is derived in (58).

Proof: On substituting (48) into (35), we have

$$\Pr\left(C_{RD}\geq R_o\right)=1-\Pr\left(\frac{1}{2}\log_2\left(\frac{1+\gamma_{RD}}{1+\gamma_{SE2}}\right)\right.$$

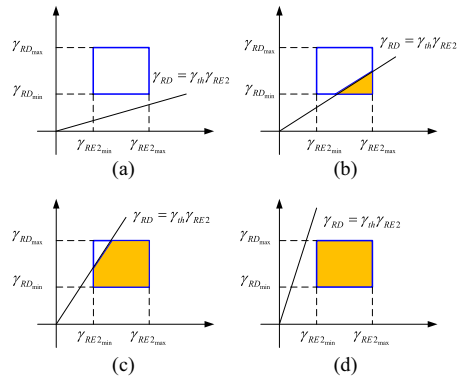

Fig. 2. Four cases of integral region of (52). (a) $\gamma_{th}\leq\gamma_{RD_{\min}}/\gamma_{RE2_{\max}}$ (b) $\gamma_{RD_{\min}}/\gamma_{RE2_{\max}}<\gamma_{th}\leq\gamma_{RD_{\min}}/\gamma_{RE2_{\min}}$ (c) $\gamma_{RD_{\max}}/\gamma_{RE2_{\max}}<\gamma_{th}<\gamma_{RD_{\max}}/\gamma_{RE2_{\min}}$ (d) $\gamma_{th}\geq\gamma_{RD_{\max}}/\gamma_{RE2_{\min}}$.

$$\left.<\frac{1}{2}\log_2\left(1+\gamma_{th}\right)\right) \tag{50}$$

In indoor VLC, it is reasonable to assume that $\gamma_{RD}>>1$ and $\gamma_{SE1}>>1$. Therefore, the upper bound on (50) is given by

$$\Pr\left(C_{RD}\geq R_o\right)\leq 1-\Pr\left(\gamma_{RD}<\gamma_{th}\gamma_{SE2}\right) \tag{51}$$

Since γ_{RD} and γ_{SE1} are independent of each other, the solution of (51) depends on γ_{th}. Therefore, we define the four different scenarios in Fig. 2 to calculate the integral regions of $\Pr(\gamma_{RD}<\gamma_{th}\gamma_{SE2})$. Based on the considered scenarios, (51) is derived as follows:

$$\Pr\left(C_{RD}\geq R_o\right)\leq\begin{cases}1, & \gamma_{th}\leq\frac{\gamma_{RD_{\min}}}{\gamma_{RE2_{\max}}}\\ 1-P_4, & \frac{\gamma_{RD_{\min}}}{\gamma_{RE2_{\max}}}<\gamma_{th}\leq\frac{\gamma_{RD_{\min}}}{\gamma_{RE2_{\min}}}\\ 1-P_5, & \frac{\gamma_{RD_{\max}}}{\gamma_{RE2_{\max}}}<\gamma_{th}<\frac{\gamma_{RD_{\max}}}{\gamma_{RE2_{\min}}}\\ 0, & \gamma_{th}\geq\frac{\gamma_{RD_{\max}}}{\gamma_{RE2_{\min}}}\end{cases}, \tag{52}$$

where

$$P_4=\int_{\frac{\gamma_{RD_{\min}}}{\gamma_{th}}}^{\gamma_{RE2_{\max}}}\int_{\gamma_{RD_{\min}}}^{\gamma_{th}z}f_{\gamma_{RE2}}\left(z\right)f_{\gamma_{RD}}\left(w\right)dwdz \tag{53}$$

$$P_5=\int_{\gamma_{RE2_{\min}}}^{\frac{\gamma_{RD_{\max}}}{\gamma_{th}}}\int_{\gamma_{RD_{\min}}}^{\gamma_{th}z}f_{\gamma_{RE2}}\left(z\right)f_{\gamma_{RD}}\left(w\right)dwdz+\int_{\frac{\gamma_{RD_{\max}}}{\gamma_{th}}}^{\gamma_{RE2_{\max}}}\int_{\gamma_{RD_{\min}}}^{\gamma_{RD_{\max}}}f_{\gamma_{RE2}}\left(z\right)f_{\gamma_{RD}}\left(w\right)dwdz \tag{54}$$

With the help of [42, Eq. (2.111.1)], the integrals in (53) and (54) are deduced as

$$P_4=\frac{\left(\mu_{RD}\mu_{RE2}\chi^4\right)^{\frac{1}{\omega+3}}}{r_\omega^4}\left\{\gamma_{RD_{\min}}^{-\frac{1}{\omega+3}}\left(\left(\frac{\gamma_{RD_{\min}}}{\gamma_{th}}\right)^{-\frac{1}{\omega+3}}-\gamma_{RE2_{\max}}^{-\frac{1}{\omega+3}}\right)\right.$$
$$\left.-\frac{\gamma_{th}^{-\frac{1}{\omega+3}}}{2}\left(\left(\frac{\gamma_{RD_{\min}}}{\gamma_{th}}\right)^{-\frac{2}{\omega+3}}-\gamma_{RE2_{\max}}^{-\frac{2}{\omega+3}}\right)\right\} \tag{55}$$

$$P_5 = \frac{\left(\mu_{RD}\mu_{RE2}\chi^4\right)^{\frac{1}{\omega+3}}}{r_\omega^4}\left\{\gamma_{RD_{\min}}^{-\frac{1}{\omega+3}}\left(\gamma_{RE2_{\min}}^{-\frac{1}{\omega+3}} - \left(\frac{\gamma_{RD_{\max}}}{\gamma_{th}}\right)^{-\frac{1}{\omega+3}}\right) - \frac{\gamma_{th}^{-\frac{1}{\omega+3}}}{2}\left(\gamma_{RE2_{\min}}^{-\frac{2}{\omega+3}} - \left(\frac{\gamma_{RD_{\max}}}{\gamma_{th}}\right)^{-\frac{2}{\omega+3}}\right)\right\} + \frac{\left(\mu_{RD}\mu_{RE2}\chi^4\right)^{\frac{1}{\omega+3}}}{r_\omega^4}\left(\gamma_{RE2_{\min}}^{-\frac{1}{\omega+3}} - \gamma_{RE2_{\max}}^{-\frac{1}{\omega+3}}\right) \times \left(\left(\frac{\gamma_{RD_{\max}}}{\gamma_{th}}\right)^{-\frac{1}{\omega+3}} - \gamma_{RE2_{\max}}^{-\frac{1}{\omega+3}}\right) \quad (56)$$

Now, by substituting (49) into (34), we obtain

$$\Pr\left(C_{SR} \geq R_o\right) = \xi - F_{\widehat{\gamma}_{SR}}\left(2^{2R_o} - 1\right) \quad (57)$$

By substituting (52) and (57) into (33), then the lower bound on SOP can be written as

$$P_{SOP}^{L}\left(R_o\right) = \begin{cases} 1 - \xi + F_{\widehat{\gamma}_{SR}}\left(2^{2R_o} - 1\right), & \gamma_{th} \leq \frac{\gamma_{RD_{\min}}}{\gamma_{RE2_{\max}}} \\ 1 - \left(\xi - F_{\widehat{\gamma}_{SR}}\left(2^{2R_o} - 1\right)\right)\left(1 - P_4\right), & \frac{\gamma_{RD_{\min}}}{\gamma_{RE2_{\max}}} < \gamma_{th} \leq \frac{\gamma_{RD_{\min}}}{\gamma_{RE2_{\min}}} \\ 1 - \left(\xi - F_{\widehat{\gamma}_{SR}}\left(2^{2R_o} - 1\right)\right)1 - P_5, & \frac{\gamma_{RD_{\max}}}{\gamma_{RE2_{\max}}} < \gamma_{th} < \frac{\gamma_{RD_{\max}}}{\gamma_{RE2_{\min}}} \\ 1, & \gamma_{th} \geq \frac{\gamma_{RD_{\max}}}{\gamma_{RE2_{\min}}} \end{cases} \quad (58)$$

Remark 9: From (58), it can be seen that SOPs with lower σ_{RE2}^2 or larger σ_{RD}^2 are higher. This is because a lower value of σ_{RE2}^2 results in a higher channel gain h_{RE2}, and a larger σ_{RD}^2 leads to a smaller channel gain h_{RD}. This can also be observed from (52) that the integral range of $\Pr(\gamma_{RD} < \gamma_{th}\gamma_{SE2})$ is enhanced for lower σ_{RE2}^2 or larger σ_{RD}^2.

Remark 10: The SOP in (58) is enlarged for larger values of γ_{th} and if $\gamma_{th} \geq \frac{\gamma_{RD_{\max}}}{\gamma_{RE2_{\min}}}$, the SOP reaches a maximum value of 1and hence information can never be transmitted securely.

Remark 11: One can derive the SOP for the case of simultaneous eavesdropping attacks on RF and VLC links by using the similar approach adopted to achieve (45) and (58). In this case, the instantaneous capacity of the corresponding links can be expressed as given in (36) and (48). Then, by substituting (41) and (51) into (33), the lower bound on SOP can easily be obtained.

V. Numerical Results and Discussions

This section presents the analytically evaluated results for the proposed dual-hop mixed RF-VLC high-speed train (HST) system with varying system parameters, such as Doppler shift and RF and VLC fading parameters, and different system configurations. Simulation results are provided for verifying the correctness of the derived results. Firstly, we examine the effect of Doppler shift and fading parameters on the proposed system's performance, followed by an analysis of its secrecy performance in the presence of eavesdroppers. The system parameters utilized in the analysis are drawn from various sources, including [15], [23], [36], [38], and are listed in Table I.

TABLE I
System Parameters for Numerical Results

Parameter	Value
f_c	5.9GHz
R_S	9.6Kbps
c	3×10^8 m/s
$\hat{r}$	0.5
σ_{SR}^2	1
Λ	1cm^2
$\Re$	0.4 A/W
T	1
ζ	1.5
η	0.8
$\phi_{1/2}$	20^0
ψ	80^0
P_{opt}	2 W
σ_{RD}^2	10^{-21} W/Hz
B	20 MHz

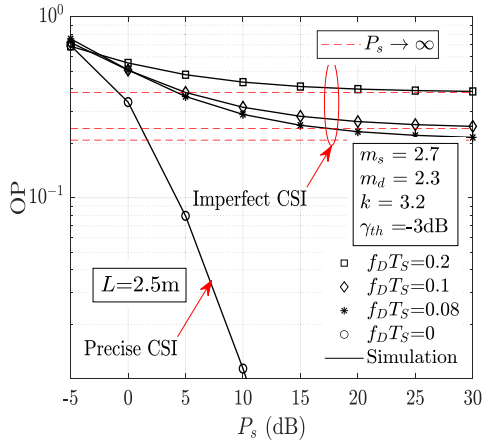

Fig. 3. OP of the mixed RF-VLC HST system vs. Transmitted power at BS.

A. Characteristics Performance of Mixed RF-VLC HST System

The outage probability of the considered system derived in (19) as a function of transmitted power at the BS under varying Doppler shift is plotted in Fig. 3. We consider four different values of Doppler shift as $\{0.2, 0.1, 0.08, 0\}$, which correspond to different train speeds $\{400, 200, 150, 0\}$ in kmph. This means that higher train speeds provide larger f_DT_S as they are related to each other as given in (3). The result clearly shows that outage is enhanced with increasing f_DT_S. This is because estimation of the fading channel at the relay is accurate at relatively smaller f_DT_S. On the other hand, larger f_DT_S leads to higher channel estimation errors, and hence the performance degrades significantly. The effect of f_DT_S can be mitigated on the cost of increasing transmitted power at BS, as shown in the result. However, the outage probability decreases to an error floor on high transmitted power due to channel estimation errors and dominance of the VLC link, which is derived in (23). Our results are consistent with the results in [3], [16], [40], [41], as the

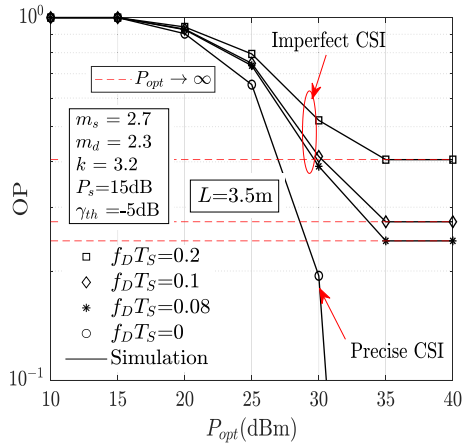

Fig. 4. OP of the mixed RF-VLC HST system vs. LED power.

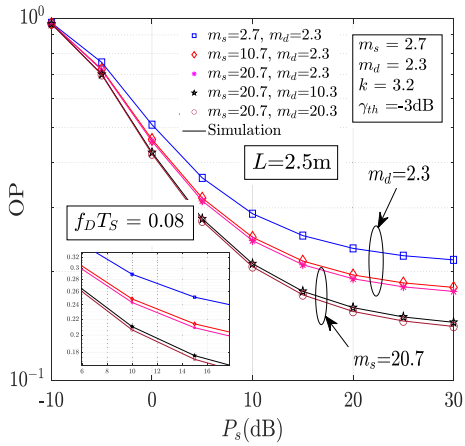

Fig. 5. OP of the mixed RF-VLC HST system under various fading conditions.

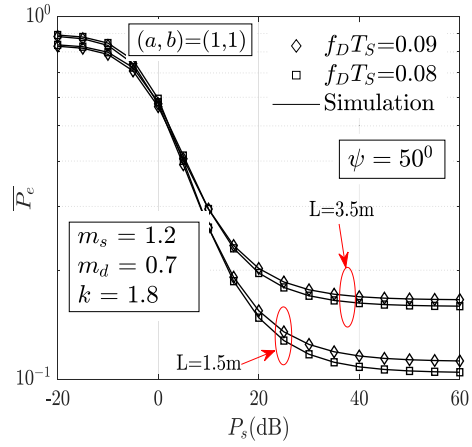

Fig. 6. Average BER of the mixed RF-VLC HST system vs. transmitted power at BS.

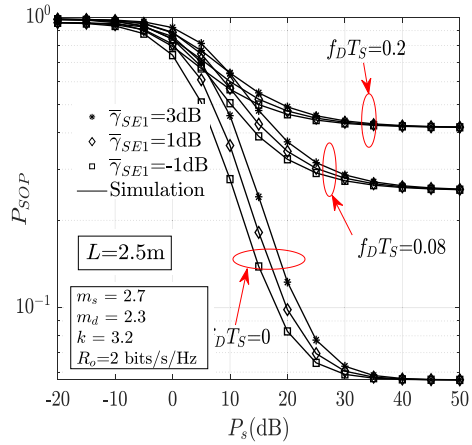

Fig. 7. bound on SOP of the mixed RF-VLC HST system under RF eavesdropping attacks.

effects of the Doppler shift on system performance in our study are similar to these studies.

Similar behavior of outage performance under varying Doppler shifts is presented in Fig. 4, which demonstrates the outage performance as a function of optical power. With increasing P_{opt}, the decrement in an outage probability is noticed. Similar to Fig. 3, an error floor is noticed for high values of optical power. Hence, further increments in optical power will not result in an improvement in system performance.

Fig. 5 depicts the outage probability for various RF fading conditions. One can see that severe fading conditions (i.e., low m_s and m_d) will result in a smaller OP, meaning better system performance, since higher m_s or m_d lead to more diversity gains. The reason for this is that scattered waves or LoS signals are perturbed and heavily shadowed at the low values of m_s or m_d. This condition may arise when the number of slow-moving vehicles or pedestrians is increased in the vicinity of BS or when BS is installed in a crowded area. It is noted that stronger scattered waves provide larger SNR at the relay and are beneficial for the enhancement of the system performance. The trend of this result is also supported by [31] and [46].

Fig. 6 illustrates the dependence of average BER on the distance between LED and receiving plane, considering different Doppler shifts. It can be observed that average BER is enlarged for higher L. This is because the larger L represents a longer path of optical signal propagation, resulting in a reduction in received power at the UE. Moreover, when the UE is closer to the relay, the BS-relay link conditions have a stronger impact on the average BER at low transmitted power at BS. Hence, a crossover point can be observed in the low transmitted power regime, while in the high transmitted power regime, the closer the UE to the relay, the less the average BER is achieved. Additionally, due to the larger channel estimation errors at the higher speed of the train, the system performance has become worse. Additionally, it is worth noting that the presence of channel estimation errors can cause the performance of the BER to converge to a discernible error floor.

B. Secrecy Performance of Mixed RF-VLC HST System

Fig. 7 shows the secrecy performance under BS-relay link eavesdropping for different values of average SNR of BS-*E1* channel as a function of transmitted power at BS. As expected, the security of the proposed system is enhanced significantly with increasing P_s or decreasing $\bar{\gamma}_{SE1}$, as testified in [30]. The reason is that the SNR at the relay is improved with increasing

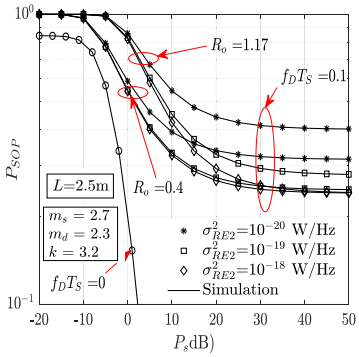

Fig. 8. Lower bound on SOP of the mixed RF-VLC HST system under VLC eavesdropping attacks.

P_s, while the SNR at the *E1* is reduced with decreasing $\bar{\gamma}_{SE1}$ due to the higher noises in the BS-*E1* link. Thus, from (36), the difference between the channel capacities of the BS-relay and BS-*E1* links is increased, and hence SOP is reduced which can be seen from (33). Another interesting observation that can be noted from the result is that a smaller Doppler shift has an insignificant impact on SOP in the low P_s regime, while SOP is enhanced with an increasing Doppler shift in the high P_s regime. This is because the difference between channel capacities of the BS-relay and BS-*E1* links is very small, with lower P_s resulting in a larger SOP.

Fig. 8 depicts the secrecy performance under relay-UE link eavesdropping for different eavesdroppers' noise and predetermined secrecy rate as a function of transmitted power at BS. We can see that the secrecy performance is improved with the increase in σ^2_{RE2}, which coincides with Remark 9. This is because a larger σ^2_{RE2} will result in a smaller SNR at the *E2*, and hence the difference between the channel capacities of relay-UE and relay-*E2* links is increased, which can be calculated from (48). This implies that the larger the noise present in the relay-E2 link leads to lower SOP as SOP depends on the difference between the channel capacities of the relay-UE and relay-*E2* links. Moreover, the secrecy performance can be improved by controlling the predetermined secrecy rate R_o, as one can easily find from (33) that a larger predetermined secrecy rate increases the chances of eavesdropping. At larger R_o, the BS has no choice other than to increase its transmission power to raise the channel capacity of the legitimate link, which may compromise the security of the system. Additionally, the impact of the Doppler shift remains similar to the previous case because channel estimation errors at the relay are forwarded the same to both UE and *E2*.

VI. Conclusion

In this work, RF and VLC technologies are combined together to support communication between a BS and a UE present on the HST, where it is assumed that the BS-relay links are subject to DSR fading while the onboard passengers are served with VLC links. The impact of the speed of HST is considered in terms of imperfect CSI at the relay, where the correlation between estimated channel gain and precise channel gain is characterized with the help of Jake's model. Particularly, a performance framework is presented to investigate the effects of the Doppler shift on HST communication. First, the statistical characteristics, including PDF and CDF, for the proposed system were derived. Subsequently, we proceeded to derive the key performance metrics, including the outage and average BER, along with the corresponding closed-form expressions for the secrecy metric, i.e., SOP, accompanied by their respective asymptotic expressions. This study highlights the advantages of using the proposed mixed RF-VLC system for dealing with future challenges in HST communication, including spectrum scarcity and eavesdropping attacks.

Appendix A

The PDF of $h_{SR}$is given by [31]

$$f_{h_{SR}}(r) = \sum_{p=0}^{\infty} \frac{A_{p_{SR}}(1+k_{SR})\,2r}{(m_{s_{SR}}-1)\,\widehat{r}^2} G_{1,1}^{1,1}\left[\frac{(1+k_{SR})\,r^2}{(m_{s_{SR}}-1)\,\widehat{r}^2}\,\middle|\,\begin{matrix}-m_{s_{SR}}\\ p\end{matrix}\right] \tag{A.1}$$

Let $X=\rho_{SR}h_{SR}$, $Y=\sqrt{1-\rho_{SR}^2}\varepsilon_{SR}$ and $Z=\widehat{h}_{SR}$, one can easily obtain the PDFs of X and Y as

$$f_X(x) = \sum_{p=0}^{\infty} \frac{A_{p_{SR}}(1+k_{SR})2x}{(m_{s_{SR}}-1)\widehat{r}^2\rho_{SR}^2} G_{1,1}^{1,1}\left[\frac{(1+k_{SR})x^2}{(m_{s_{SR}}-1)\widehat{r}^2\rho_{SR}^2}\,\middle|\,\begin{matrix}-m_{s_{SR}}\\ p\end{matrix}\right] \tag{A.2}$$

$$f_Y(y) = \frac{1}{\sqrt{2\pi\,(1-\rho_{SR}^2)}} \exp\left(\frac{-y^2}{2\,(1-\rho_{SR}^2)}\right) \tag{A.3}$$

Based on convolution theorem, the PDF of Z can be written as

$$f_{\widehat{h}_{SR}}(z) = \int_0^{\infty} f_X(x) f_Y(z-x)\,dx = \sum_{p=0}^{\infty} \frac{A_{p_{SR}}(1+k_{SR})}{(m_{s_{SR}}-1)\,\widehat{r}^2\rho_{SR}^2\sqrt{2\pi\,(1-\rho_{SR}^2)}}\Delta(z) \tag{A.4}$$

where

$$\Delta(z) = \int_0^{\infty} 2x G_{1,1}^{1,1}\left[\frac{(1+k_{SR})\,x^2}{(m_{s_{SR}}-1)\,\widehat{r}^2\rho_{SR}^2}\,\middle|\,\begin{matrix}-m_{s_{SR}}\\ p\end{matrix}\right] \times \exp\left(\frac{-(z-x)^2}{2\,(1-\rho_{SR}^2)}\right) dx \tag{A.5}$$

Representing $\exp(-x)$ into Meijer's G function from [36, (8.4.3.1)] and using $e^x=\sum_{n=0}^{\infty}\frac{x^n}{\Gamma(n+1)}$, we obtain the solution of (A.5) with the help of [37, (07.34.21.0011.01)] as

$$\Delta(z) = \sum_{q=0}^{\infty} \frac{z^q 2^{q/2+1} G_{pq}}{\Gamma(q+1)\,(1-\rho_{SR}^2)^{q/2-1}} \exp\left(-\frac{z^2}{2\,(1-\rho_{SR}^2)}\right) \times G_{2,1}^{1,2}\left[\frac{(1+k_{SR})\,2\,(1-\rho_{SR}^2)}{(m_{s_{SR}}-1)\,\widehat{r}^2\rho_{SR}^2}\,\middle|\,\begin{matrix}-m_{s_{SR}}, -q/2\\ p\end{matrix}\right] \tag{A.6}$$

Substituting (A.6) into (A.4), we have

$$f_{\hat{h}_{SR}}(z) = \sum_{\infty}^{\infty}\sum_{\infty}^{\infty} \frac{A_{p_{SR}} z^q 2^{q/2-1/2} G_{pq}}{\sqrt{\pi}\Gamma(q+1)\left(1-\rho_{SR}^2\right)^{q/2+1/2}} \times \exp\left(-\frac{z^2}{2\left(1-\rho_{SR}^2\right)}\right) \tag{A.7}$$

where $G_{pq} = G_{2,1}^{1,2}\left[\frac{(1+k_{SR})2(1-\rho_{SR}^2)}{(m_{s_{SR}}-1)\widehat{r}^2\rho_{SR}^2}\middle| \begin{matrix} -m_{s_{SR}}+1, -q/2+1 \\ p+1 \end{matrix}\right]$.

In practical fading models, the channel gain coefficients must be positive. Keeping this in mind, we can rewrite (A.7) as

$$f_{\hat{h}_{SR}}(z) = \begin{cases} \sum_{\infty}^{\infty}\sum_{\infty}^{\infty} \frac{A_{p_{SR}} z^q 2^{q/2-1/2} G_{pq}}{\sqrt{\pi}\Gamma(q+1)\left(1-\rho_{SR}^2\right)^{q/2+1/2}} \exp\left(-\frac{z^2}{2\left(1-\rho_{SR}^2\right)}|!\right), & z>0 \\ 1-\xi, & z=0 \end{cases} \tag{A.8}$$

With the help of [38, Eq. (3.326.2)] and using $\int_0^{\infty} f_{h_{SR}}(z)dz = 1$, ξ can be obtained as

$$\xi = \sum_{p=0}^{\infty}\sum_{q=0}^{\infty} \frac{A_{p_{SR}} 2^{q-1}}{\sqrt{\pi}\Gamma(q+1)} G_{pq}\Gamma\left(\frac{q+1}{2}\right) \tag{A.9}$$

Finally, using change of variable based on (4), we obtain the PDF in (5) and then the CDF is obtained in (6) using [38, Eq. (07.34.21.0084.01)].

Appendix B

According to d'Alembert's ratio test, any infinite series $\sum_{i,j} a_i b_j$ is convergent if

$$\lim_{\substack{i\to\infty \\ j\to\infty}} \left|\frac{a_{i+1}b_{j+1}}{a_i b_j}\right| < 1 \tag{A.10}$$

The $i$thand jth terms in the series expansion of CDF of DSR distribution are

$$a_i = \frac{A_{i_{SR}} 2^{j-1} G_{ij}}{\sqrt{\pi}\Gamma(j+1)} \tag{A.11}$$

$$b_j = G_{1,2}^{1,1}\left[\Omega\gamma\middle| \begin{matrix} 1 \\ \frac{j+1}{2} \end{matrix}, 0\right] \tag{A.12}$$

Therefore,

$$\frac{a_{i+1}b_{j+1}}{a_i b_j} = \frac{\frac{A_{i+1_{SR}} 2^j G_{i+1j+1}}{\sqrt{\pi}\Gamma(j+2)} G_{1,2}^{1,1}\left[\Omega\gamma\middle| \begin{matrix} 1 \\ \frac{j+2}{2} \end{matrix}, 0\right]}{\frac{A_{i_{SR}} 2^{j-1} G_{ij}}{\sqrt{\pi}\Gamma(j+1)} G_{1,2}^{1,1}\left[\Omega\gamma\middle| \begin{matrix} 1 \\ \frac{j+1}{2} \end{matrix}, 0\right]} \tag{A.13}$$

It is well-known that for any values of i, j, the ratio of two Meijer-G functions will always be a non-zero real number. Therefore, (A.13) can be written as

$$\frac{a_{i+1}b_{j+1}}{a_i b_j} = \frac{A_{i+1_{SR}} 2\Gamma(j+1)}{A_{i_{SR}}\Gamma(j+2)}\theta_1\theta_2 \tag{A.14}$$

where $\theta_1 = \frac{G_{1,2}^{1,1}\left[\Omega\gamma\middle| \begin{matrix} 1 \\ \frac{j+2}{2} \end{matrix}, 0\right]}{G_{1,2}^{1,1}\left[\Omega\gamma\middle| \begin{matrix} 1 \\ \frac{j+1}{2} \end{matrix}, 0\right]}$ and $\theta_2 = \frac{G_{i+1j+1}}{G_{ij}}$.

It can be seen from (A.14) that the order of i, j in the denominator is greater than the order of i, j in the numerator, which provides 0 on applying the $i \to \infty, j \to \infty$.

References

[1] J. Kim et al., "A comprehensive study on mmWave-based mobile hotspot network system for high-speed train communications," *IEEE Trans. Veh. Technol.*, vol. 68, no. 3, pp. 2087–2101, Mar. 2019.

[2] M. Zhu, Y. Wang, X. Liu, S. Ma, X. Zhang, and Y. Fu, "Performance analysis for DF relay-aided visible light communication system with NOMA," *IEEE Photon. J.*, vol. 14, no. 5, Oct. 2022, Art. no. 7350809.

[3] F. Baklouti, I. Dayoub, S. Haxha, R. Attia, and A. Aggoun, "Novel method for improving the capacity of optical MIMO system using MGDM," *IEEE Photon. J.*, vol. 6, no. 6, Dec. 2014, Art. no. 7903515.

[4] S. Han et al., "Achieving high spectrum efficiency on high speed train for 5G new radio and beyond," *IEEE Wireless Commun.*, vol. 26, no. 5, pp. 62–69, Oct. 2019.

[5] E. Yaacoub, R. Atat, A. Alsharoa, and M. S. Alouini, "Mobile relays for enhanced broadband connectivity in high speed train systems," *Phys. Commun.*, vol. 12, pp. 105–115, Jun. 2014.

[6] B. Ai et al., "Future railway services-oriented mobile communications network," *IEEE Commun. Mag.*, vol. 53, no. 10, pp. 78–85, Oct. 2015.

[7] R. He et al., "Propagation channels of 5G millimeter-wave vehicle-tovehicle communications: Recent advances and future challenges," *IEEE Veh. Technol. Mag.*, vol. 15, no. 1, pp. 16–26, Mar. 2020.

[8] R. He, B. Ai, G. L. Stuber, G. Wang, and Z. Zhong, "Geometrical-based modeling for millimeter-wave MIMO mobile-to-mobile channels," *IEEE Trans. Veh. Technol.*, vol. 67, no. 4, pp. 2848–2863, Apr. 2018.

[9] C. Huang, A. F. Molisch, Y.-A. Geng, R. He, B. Ai, and Z. Zhong, "Trajectory-joint clustering algorithm for time-varying channel modeling," *IEEE Trans. Veh. Technol.*, vol. 69, no. 1, pp. 1041–1045, Jan. 2020.

[10] K. Guan et al., "Towards realistic high-speed train channels at 5G millimeter-wave band—Part I: Paradigm, significance analysis, and scenario reconstruction," *IEEE Trans. Veh. Technol.*, vol. 67, no. 10, pp. 9112–9128, Oct. 2018.

[11] K. Guan et al., "Towards realistic high-speed train channels at 5G millimeter-wave band—Part II: Case study for paradigm implementation," *IEEE Trans. Veh. Technol.*, vol. 67, no. 10, pp. 9129–9144, Oct. 2018.

[12] J. Yang et al., "An efficient MIMO channel model for LTE-R network in high-speed train environment," *IEEE Trans. Veh. Technol.*, vol. 68, no. 4, pp. 3189–3200, Apr. 2019.

[13] L. Wang, B. Ai, Y. Niu, X. Chen, and P. Hui, "Energy-efficient power control of train-ground mmWave communication for high-speed trains," *IEEE Trans. Veh. Technol.*, vol. 68, no. 8, pp. 7704–7714, Aug. 2019.

[14] P. Agheli, H. Beyranvand, and M. J. Emadi, "High-speed trains access connectivity through RIS-assisted FSO communications," *J. Lightw. Technol.*, vol. 40, no. 21, pp. 7084–7094, Nov. 2022, doi: 10.1109/JLT.2022.3199608.

[15] M. T. Dabiri, S. M. S. Sadough, and M. A. Khalighi, "FSO communication for high speed trains: Blind data detection and channel estimation," in *Proc. 11th Int. Symp. Commun. Syst., Netw. Digit. Signal Process.*, 2018, pp. 1–4.

[16] H. S. Khallaf and M. Uysal, "UAV-based FSO communications for high speed train backhauling," in *Proc. IEEE Wireless Commun. Netw. Conf.*, 2019, pp. 1–6.

[17] H. S. Khallaf and M. Uysal, "Comprehensive study on UAV-based FSO links for high-speed train backhauling," *Appl. Opt.*, vol. 60, no. 27, pp. 8239–8247, 2021.

[18] Z. Ghassemlooy, W. Popoola, and S. Rajbhandari, *Optical Wireless Communications: System and Channel Modelling With MATLAB*. Boca Raton, FL, USA: CRC Press, 2013.

[19] S. Wu, H. Wang, and C.-H. Youn, "Visible light communications for 5G wireless networking systems: From fixed to mobile communications," *IEEE Netw.*, vol. 28, no. 6, pp. 41–45, Nov./Dec. 2014.

[20] W. A. W. M. Mahyiddin, P. A. Martin, and P. J. Smith, "Massive MIMO systems in time-selective channels," *IEEE Commun. Lett.*, vol. 19, no. 11, pp. 1973–1976, Nov. 2015.

[21] M. M. Taygur and T. F. Eibert, "Analyzing the channel aging effects on massive MIMO downlink by ray-tracing," in *Proc. IEEE 29th Annu. Int. Symp. Pers., Indoor Mobile Radio Commun.*, 2018, pp. 1–5.

[22] K. S. Gomadam and S. A. Jafar, "Impact of mobility on cooperative communication," in *Proc. IEEE Wireless Commun. Netw. Conf.*, 2006, pp. 908–913.

[23] A. Al-Rimawi, J. Siam, and A. Abdo, "The outage probability of mobile wireless networks over η-μ fading channel," in *Proc. IEEE Middle East North Afr. Commun. Conf.*, 2018, pp. 1–5.

[24] M. I. Petkovic, A. M. Cvetkovic, M. Narandzic, N. D. Chatzidiamantis, D. Vukobratovic, and G. K. Karagiannidis, "Mixed RF-VLC relaying systems for interference-sensitive mobile applications," *IEEE Trans. Veh. Tech.*, vol. 69, no. 10, pp. 11099–11111, Oct. 2020.

[25] C. Mukasa, V. A. Aalo, and G. Efthymoglou, "On the performance of a dual-hop network with a mobile relay in a Nakagami fading environment," in *Proc. 21st Int. Workshop Comput. Aided Model. Des. Commun. Links Netw.*, 2016, pp. 43–47.

[26] W. Zeng, J. Zhang, K. P. Peppas, B. Ar, and Z. Zhong, "UAVaided wireless information and power transmission for high-speed train communications," in *Proc. 21st Int. Conf. Intell. Transp. Syst.*, 2018, pp. 3409–3414.

[27] ERTMS/ETCS - Class 1, "Subset-037 euroradio FIS," Oct. 2005. Accessed: Apr. 2, 2023. [Online]. Available: https://www.era.europa.eu/system/files/2023-01/sos1_index039_-_subset-092-1_v230.pdf

[28] J. Hyun-Jeong, H. Jong-Gyu, S. Seung-Kwon, and K. Yong-Kyu, "Safety guaranteeing method & tool development in railway communication system," in *Proc. 31st Int. Telecommun. Energy Conf.*, 2009, pp. 1–5.

[29] Y. Wang, Y. Tong, and Z. Zhan, "On secrecy performance of mixed RF-FSO systems with a wireless-powered friendly jammer," *IEEE Photon. J.*, vol. 14, no. 2, Apr. 2022, Art. no. 7314708.

[30] M. J. Saber, A. Keshavarz, J. Mazloum, A. M. Sazdar, and M. J. Piran, "Physical-layer security analysis of mixed SIMO SWIPT RF and FSO fixed-gain relaying systems," *IEEE Syst. J.*, vol. 13, no. 3, pp. 2851–2858, Sep. 2019.

[31] R. Singh, M. Rawat, and A. Jaiswal, "On the performance of mixed FSO/RF SWIPT systems with secrecy analysis," *IEEE Syst. J.*, vol. 16, no. 1, pp. 339–350, Mar. 2022.

[32] J. Liu, J. Wang, B. Zhang, and Q. Wang, "Secrecy performance analysis of hybrid RF/VLC dual-hop relaying systems," *Front. Phys.*, vol. 9, Jul. 2021, Art. no. 683479.

[33] J. Qiao, X. Zhao, and Y. Sun, "On the physical layer security of multi-user hybrid RF/VLC networks," in *Proc. 13th Int. Conf. Commun. Softw. Netw.*, 2021, pp. 11–16.

[34] W. Zhang, X. Zhao, and G. Jiang, "Physical layer security for intelligent reflecting surface-assisted VLC/RF hybrid network," in *Proc. 14th Int. Conf. Commun. Softw. Netw.*, 2022, pp. 23–27.

[35] G. Pan, J. Ye, and Z. Ding, "Secure hybrid VLC-RF systems with light energy harvesting," *IEEE Trans. Commun.*, vol. 65, no. 10, pp. 4348–4359, Oct. 2017, doi: 10.1109/TCOMM.2017.2709314.

[36] Z. Liao, L. Yang, J. Chen, H.-C. Yang, and M.-S. Alouini, "Physical layer security for dual-hop VLC/RF communication systems," *IEEE Commun. Lett.*, vol. 22, no. 12, pp. 2603–2606, Dec. 2018.

[37] G. Pan et al., "Secure cooperative hybrid VLC-RF systems," *IEEE Trans. Wireless Commun.*, vol. 19, no. 11, pp. 7097–7107, Nov. 2020.

[38] C. Yaping and X. Fang, "A physical layer secure wireless communication scheme for high speed railway," in *Proc. 6th Int. Workshop Signal Des. Appl. Commun.*, 2013, pp. 114–117.

[39] W. Xie et al., "Secrecy performance analysis of the NOMA system on high-speed railway," *Secur. Commun. Netw.*, vol. 2020, Dec. 2020, Art. no. 8868550.

[40] A. Prudnikov, Y. Brychkov, and O. Marichev, *Integrals and Series: More Special Functions*. vol. 3. Philadelphia, PA, USA: Gordon And Breach Science Publishers, 1992.

[41] Wolfram, "The wolfram functions site," Accessed: Apr. 20, 2023. [Online]. Available: http://functions.wolfram.com/id

[42] I. Gradshteyn and I. Ryzhik, *Table of Integrals, Series and Products*. 7th ed. New York, NY, USA: Academic, 2007.

[43] N. Yang, M. Elkashlan, P. L. Yeoh, and J. Yuan, "Multiuser MIMO relay networks in Nakagami-m fading channels," *IEEE Trans. Commun.*, vol. 60, no. 11, pp. 3298–3310, Nov. 2012.

[44] J. Zhang, H. Du, P. Zhang, J. Cheng, and L. Yang, "Performance analysis of 5G mobile relay systems for high-speed trains," *IEEE J. Sel. Areas Commun.*, vol. 38, no. 12, pp. 2760–2772, Dec. 2020.

[45] J. Zhao, J. Wu, and P. Fan, "Performance analysis for high-speed railway distributed antenna systems with imperfect channel state information," *J. Wireless Commun. Netw.*, vol. 2018, Dec. 2018, Art. no. 275.

[46] R. Singh, M. Rawat, and A. Jaiswal, "On the physical layer security of mixed FSO-RF SWIPT system with non-ideal power amplifier," *IEEE Photon. J.*, vol. 13, no. 4, Aug. 2021, Art. no. 7300517.